Liu *et al. Microbiome* (2025) 13:111
https://doi.org/10.1186/s40168-025-02103-z

Microbiome

RESEARCH

Open Access

Microbe-mediated stress resistance in plants: the roles played by core and stress-specific microbiota

Sijia Liu[1,2,3†], Jiadong Wu[1,2,3†], Zhen Cheng[1,2,3†], Haofei Wang[1,2,3], Zhelun Jin[1,2,3], Xiang Zhang[1,2,3], Deqiang Zhang[1,2,3] and Jianbo Xie[1,2,3*]

Abstract

Background Plants in natural surroundings frequently encounter diverse forms of stress, and microbes are known to play a crucial role in assisting plants to withstand these challenges. However, the mining and utilization of plant-associated stress-resistant microbial sub-communities from the complex microbiome remains largely elusive.

Results This study was based on the microbial communities over 13 weeks under four treatments (control, drought, salt, and disease) to define the shared core microbiota and stress-specific microbiota. Through co-occurrence network analysis, the dynamic change networks of microbial communities under the four treatments were constructed, revealing distinct change trajectories corresponding to different treatments. Moreover, by simulating species extinction, the impact of the selective removal of microbes on network robustness was quantitatively assessed. It was found that under varying environmental conditions, core microbiota made significant potential contributions to the maintenance of network stability. Our assessment utilizing null and neutral models indicated that the assembly of stress-specific microbiota was predominantly driven by deterministic processes, whereas the assembly of core microbiota was governed by stochastic processes. We also identified the microbiome features from functional perspectives: the shared microbiota tended to enhance the ability of organisms to withstand multiple types of environmental stresses and stress-specific microbial communities were associated with the diverse mechanisms of mitigating specific stresses. Using a culturomic approach, 781 bacterial strains were isolated, and nine strains were selected to construct different SynComs. These experiments confirmed that communities containing stress-specific microbes effectively assist plants in coping with environmental stresses.

Conclusions Collectively, we not only systematically revealed the dynamics variation patterns of rhizosphere microbiome under various stresses, but also sought constancy from the changes, identified the potential contributions of core microbiota and stress-specific microbiota to plant stress tolerance, and ultimately aimed at the beneficial microbial inoculation strategies for plants. Our research provides novel insights into understanding the microbe-mediated stress resistance process in plants.

Keywords Core microbiota, Stress-specific microbiota, Community ecology, Stress resistance, Metagenomic

† Sijia Liu, Jiadong Wu and Zhen Cheng contributed equally to this work.

*Correspondence:
Jianbo Xie
jbxie@bjfu.edu.cn
Full list of author information is available at the end of the article

Background

Owing to their sessile lifestyle, plants are constantly exposed to diverse biotic and abiotic stresses. Well-structured and regulated microbes establish a subtle yet relatively symbiotic relationship with plants [1, 2], assisting them in coping with challenges such as nutrient acquisition, novel and often-stressful conditions, and pathogens [3]. Recent studies have demonstrated the critical role of rhizosphere microbes in plant health and adaptation to various environmental challenges. Different microbes exhibit distinct functions in stress responses. Moreover, the microbes recruited by plants have a strong correlation with their native soil. Therefore, comprehending the variation patterns and enrichment of microbial communities under different stresses in the same soil environment provides valuable insights into microbe-mediated stress resistance and possesses significant ecological and agricultural significance.

A group of microbes that can consistently occur in the rhizosphere is defined as the core microbiota [4]. The majority of these microbes belong to abundant taxa, and their presence is closely associated with the dynamic alterations of ecosystem functions [5, 6]. In extreme environments involving drought, salinity, and disease, these microbes can still survive, fully indicating the strong viability of this group. Precisely owing to this strong adaptability, they play the role of mainstays in the complex and variable environment, which clearly shows their irreplaceable position in the ecosystem. Nevertheless, a large number of current studies have demonstrated that under stressed conditions, plants will actively recruit beneficial microbial communities in order to assist themselves in withstanding stress [7–9]. This unique phenomenon cannot be fully and profoundly revealed by exclusively depending on the definition of the core microbiota. Hence, it is imperative for us to introduce the concept of stress-specific microbiota, which are defined as microbial taxa specifically present in various distinct stress environments, so as to more precisely and comprehensively explain the interaction mechanism between plants and microbes in stressed environments. Ultimately, we need to explore the dynamic changes of microbial communities from the macroscopic perspective of the overall community; and from the relatively microscopic perspective of sub-communities, conduct an in-depth exploration of the relatively stable members and seek to discover the specific correlations within the microbial community, and subsequently analyze the distinctive roles played by the core microbiota and the stress-specific microbiota in stress events respectively.

As a model tree species, members of the *Populus* genus, characterized by their rapid growth and perennial nature, have a closer relationship with microbes, making them an attractive system for studying microbial intervention strategies. The three common stresses, namely drought, salt, and disease, are the primary stressors that poplar trees confront [10–12]. They pose substantial threats to poplar's growth and development, influencing various physiological and biochemical processes. Here, with poplar as the research material, we carried out a large-scale controlled experiment, integrated amplicon and metagenomic data, and studied and compared the bulk and rhizosphere microbiomes of poplar under normal growth conditions and the three stresses. The aims of this study were to (i) delineate the variation patterns of the microbiome in different growth states, (ii) demonstrate the functional characteristics of the microbiome under different stresses and furnish functional-level evidence for a deeper understanding of the interaction between microbes and plants, (iii) explore the roles played by the core and stress-specific microbiomes in ecosystems, and (iv) construct SynComs to enhance plant stress resistance, offering a theoretical basis for constructing an efficient plant–microbe stress resistance system. This study provides novel insights into understanding the microbe-mediated stress resistance process in plants.

Results

Uncovering alterations of the poplar microbiome under three stresses

To determine how the three stresses (drought, salt, disease) impacted microbiome recruitment, a large-scale controlled experiment was conducted to observe the relevant characteristics of the microbiome in the *Populus alba*×*P. glandulosa* (84 K) planting device from samples collected over the subsequent 13 weeks (TP1–TP13) under normal growth conditions and three stress treatments (Fig. 1). The 13-week treatment resulted in reductions in stem height (15.73%, 21.35%, and 34.83%), leaf number (22.22%, 33.33%, and 40.74%), and aboveground biomass (12.5%, 28.83%, and 32.5%) for the disease, drought, and salt treatment groups, respectively (Additional file 1: Fig. S1). According to the 16S rRNA gene amplicon sequencing results, a total of 19,548,080 high-quality bacterial reads were obtained from 312 soil samples. After removing the low-quality and plant-derived reads, the remaining reads were clustered into 8347 bacterial ASVs, which were distributed in 45 phyla and 120 classes. The 5546 ASVs were shared among all treatments, while the numbers of unique ASVs in control, drought, salt, and disease groups were 68, 95, 116, and 195, respectively (Additional file 1: Fig. S2).

In contrast to the relatively stable alterations observed in Shannon's diversity index of bulk soil samples, the rhizosphere samples displayed more pronounced variations (Fig. 2A). This suggests that the response of

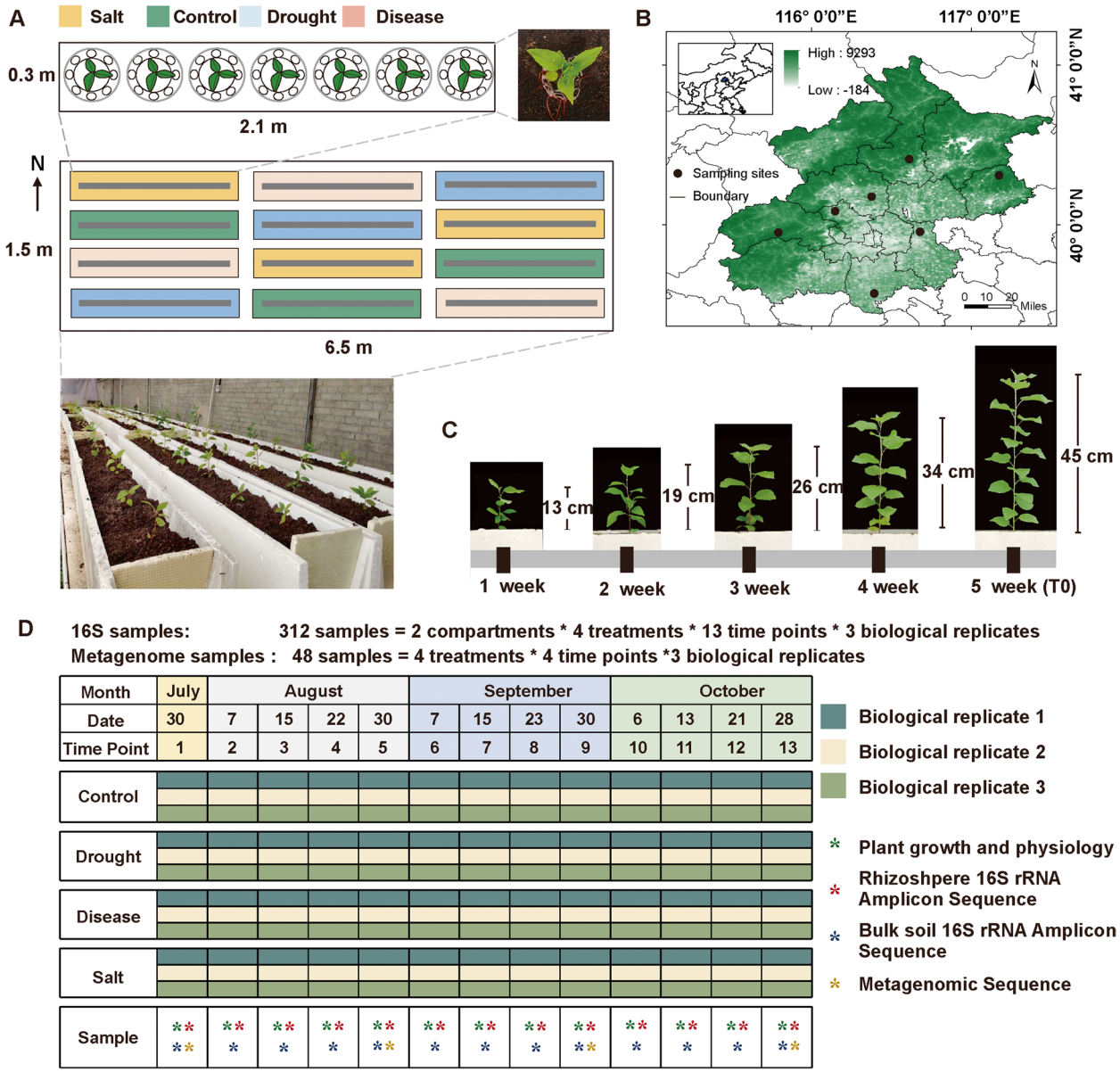

Fig. 1 Outline of the experimental design of the study. **A** Field layout of the 12 planting tanks (2.1 × 0.3 m 2 each) in a random block design of four treatments (green: control, blue: drought, yellow: salt and pink: disease) with three replicates in a 6.5 × 1.5 m 2 field. Seven groups of semi-open mesocosm were evenly spaced within each planting tank. The semi-open mesocosm system consisted of an inner reticular container and seven outer reticular containers. The inner container (root compartment) was made of the 150-μm nylon mesh net with a height of 20 cm and a diameter of 6 cm, which allowed microbes to pass freely and prevented the root from spreading and growing at will. The outer container (rhizosphere soil compartment) was the rectangular 150-μm nylon mesh bag with a height of 20 cm and a width of 2 cm. The entire semi-open ecosystem was placed in the planting tank and covered with about 3 cm of soil. **B** Collection sites of natural soils in Beijing city. The black dots were the locations for natural soil sampling. **C** The growth of plants before stress treatments. 1 week: the first week of seedings moving into the planting tanks; 2 week: the second week of seedings moving into the planting tanks; 3 week: the third week of seedings moving into the planting tanks; 4 week: the fourth week of seedings moving into the planting tanks; 5 week (T0): the fifth week of seedings moving into the planting tanks, which was the beginning of the stress treatments. **D** Sampling strategy of the experiment. Bulk soil was collected from three locations in each planting tank every week, and three outer containers were randomly collected from each semi-open ecosystem to sample the rhizosphere soil. Record the growth and physiology of plants every week

rhizosphere microbial communities to stress environments was rapid and profound [13–15]. Consequently, in the subsequent analyses, we primarily focused on the rhizosphere samples as they provide valuable insights into the ecological dynamics and responses within this crucial microenvironment. Compared to the control group, Shannon's diversity in rhizosphere samples exhibited a persistent decline trend under the three stress treatments, with significant differences observed at time points T3, T5, and T7, respectively ($P < 0.01$, Fig. 2A). In order to determine the main factors driving community composition, unconstrained principal coordinate analyses (PCoAs) of Bray Curtis distances were performed using all available ASVs. The analysis conducted on all samples revealed that the samples belonging to rhizosphere and bulk soils clustered into distinct groups (Fig. 2C), with the composition of rhizosphere soil communities exhibiting a larger combined variation being explained by the first two axes in the PCoA plots compared to bulk soil samples (rhizosphere = 31.892%, bulk soil = 21.468%, $R^2 = 0.27$, $P < 0.001$) (Additional file 1: Fig. S3, Additional file 2: Table S1). Individual PCoA analysis performed separately for each treatment type demonstrated that the stress treatment communities displayed larger and more dynamic changes, with greater separation between time points (Control: $R^2 = 0.08$, $P = 0.161$; Drought: $R^2 = 0.35$, $P < 0.001$; Disease: $R^2 = 0.19$, $P < 0.001$; Salt: $R^2 = 0.23$, $P < 0.001$) (Fig. 2D).

To further gain a comprehensive insight into the alterations in root-associated microbial communities induced by stress, we attempted to perform differential analysis of the relative abundance at different taxonomic levels to identify bacterial lineages enriched under each stress treatment. Specifically, at the phylum or class level, the salt stress and drought stress treatment groups were enriched in Firmicutes (11.32%, $P < 0.01$; 3.04%, $P < 0.01$) and Actinobacteria (6.04%, $P < 0.01$; 8.11%, $P < 0.01$), whereas the disease group was enriched in the Alpha- (36.84%, $P < 0.01$) and Gamma-proteobacteria (18.70%, $P < 0.01$) (Fig. 2B, Additional file 1: Fig. S4, Additional file 2: Table S2). Among the genera showing significant differences between the stress treatment and control groups for drought, salt, and disease (specifically 170, 154, and 180, respectively), 42.4%, 28.0%, and 36.7% of the genera exhibited strong enrichment in the stress-treated groups (Additional file 1: Fig. S5), with phylogenetic reconstruction suggesting a non-random distribution of this enrichment (Fig. S6 A). The proportion of ASVs enriched in drought, salt, and disease treatment accounted for 3.1%, 0.9%, and 3.0% of the total ASVs. Taken together, these results depicted the alteration patterns of the microbiome under different growth states and suggest different stresses exert varying pathways and time scales in influencing rhizosphere bacterial communities.

Using a Random Forest model, we identified a set of biomarker taxa that were most sensitive to stress types (Fig. 2E). After modeling the species abundance at various taxonomic levels, it was discovered that constructing the model at the family level achieved the highest accuracy, explaining 87.2% of the variation in the rhizosphere microbial community associated with stress types. To reveal important bacterial classes as biomarker taxa to correlate with stress types, we performed tenfold cross-validation with five repeats to evaluate the importance of bacterial class (Additional file 2: Table S3). The error curve stabilized with the involvement of the 22 most sensitive classes and these 22 stress-discriminant classes, belonging to 9 phyla, were determined as the biomarker taxa of the changes in stress types (Fig. 2E, Additional file 2: Table S4). Of the identified biomarker taxa, 11 were stress colonizers (stress enriched), 9 were non-stress colonizers (stress depleted), and 2 were complex colonizers (Fig. 2F). With three stress colonizers (Actinobacteria, Clostrida, and Bacilli) ranking among the top four classes in terms of importance to the model accuracy, the stress colonizers exhibited a greater contribution to the predictive model compared to the non-stress colonizers.

Identification of the core and stress-specific ASVs groups

Expanding upon the findings of differential analysis, we conducted additional investigations to discern specific rhizosphere ASVs that exhibited alterations under distinct stress conditions. Applying consistent filtering criteria, three sets of stress-specific ASVs were identified: drought-specific ASVs were predominantly concentrated

(See figure on next page.)

Fig. 2 Taxonomic distribution and diversity comparisons in rhizosphere and bulk soil microbiomes. **A** Mean Shannon's diversity index across the bulk soil and rhizosphere at each time point. All time points (T1–T13) are arranged in order along the x axis in each panel. The vertical dashed lines in the figure indicate the time points that show significant differences from the control group ($P < 0.01$). **B** Relative abundance for the most abundant bacterial phyla. Percent relative abundance of the top 10 most abundant phyla for control, drought, salt, and disease treatments across bulk soil and rhizosphere. **C** PCoA of Bray Curtis distance for all samples. Red: rhizosphere samples; blue: bulk soil samples. **D** PCoA of Bray Curtis distance for four treatment of rhizosphere samples colored by time point. Individual time points are represented by distinct colors. **E** The biomarker taxa listed in descending order of importance to the model accuracy. **F** Dynamics of the relative abundance of the stress-discriminant biomarker taxa with treatment time.

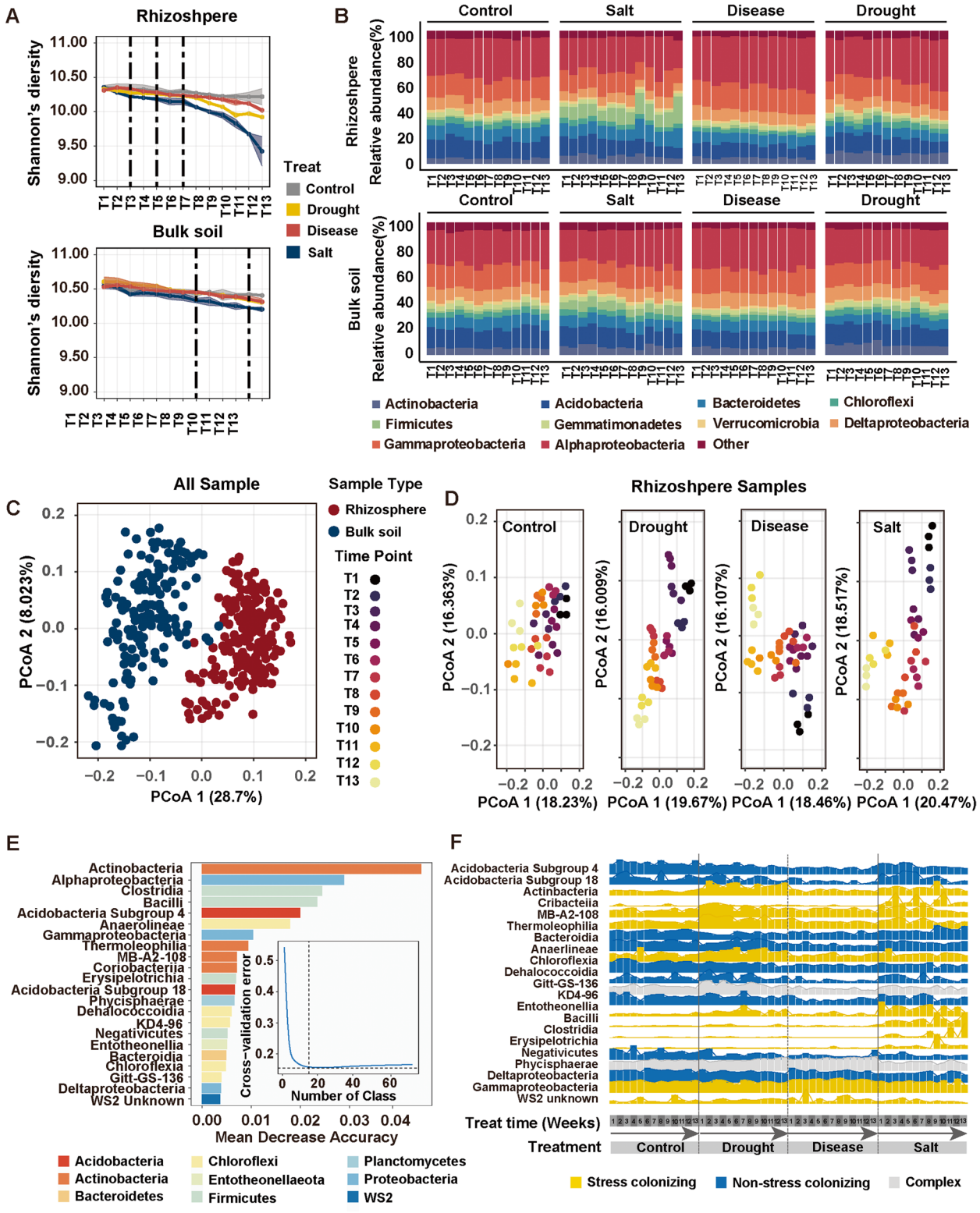

Fig. 2 (See legend on previous page.)

in Actinobacteria (48.2%) and Alphaproteobacteria (36.5%); salt-specific ASVs were primarily composed of Firmicutes (16.7%) and Actinobacteria (57.7%); disease-specific ASVs were mainly represented by Proteobacteria (70.1%) and Actinobacteria (11.4%) (Fig. S6 A). The drought, salt, and disease groups have 255, 254, and 79 ASVs respectively, with 120, 132, and 62 genera respectively. Considering the specific classification types of these ASVs, it was observed that the unique ASVs associated with each stress type (drought, salt, disease) collectively accounted for the majority, representing 68.8%, 83.8%, and 70.7% of the respective stress-specific classified bacterial ASVs (Additional file 1: Fig. S7). The enriched ASVs within each treatment displayed minimal overlap, underscoring the plants' recruitment of distinct bacterial species in response to various stresses.

In contrast to the stress-specific ASVs, which were rare and not persistent, most of the highly abundant and prevalent ASVs were shared. We proposed that a set of ASVs persisting across time and treatment groups may play unique roles in plant–microbe interactions. ASVs with a relative abundance >0.01% and present in more than 90% of the samples were defined as core microbes. A total of 126 ASVs were denoted as the core microbiota, accounting for only 1.5% of all observed ASVs but contributing 15.6% to the total beta diversity (Fig. S6B-D). A minimal overlap was observed between core and stress-specific microbiota across treatments. Specifically, only 2.4% (6 out of 255) of drought-specific microbes, 4.3% (11 out of 254) of disease-specific microbes, and 2.5% (2 out of 79) of salt-specific microbes overlapped with the core ASVs (Fig. S7). Members of the core microbiota, such as *Arthrobacter* [16], *Streptomyces* [17, 18], *Sphingobium* [19], *Bradyrhizobium* [20], and *Burkholderiales* [21], have been found to be multi-functional in the environment. Although the core microbiota primarily consists of beneficial functional bacteria, their overall functional roles in response to stress remain unclear.

Distinct co-occurrence networks of four treatments

In order to visually observe the interactions and environmental preferences among microbial species, we inferred co-occurrence patterns using metacommunity network inference based on strong and significant correlation relationships. We obtained four large networks classified by different treatments (control; drought; salt; disease), each of which was modeled as an undirected graph composed of nodes and edges. At a high level, differences in the structure of the four networks were apparent. A higher number of nodes and edges were recorded in stress networks than the control network (Fig. 3A–C, Additional file 2: Table S5), creating more intricate network patterns, which supports our expectation that potential interactions in stress networks are stronger than those of the control network. The average degree and the average clustering coefficient of networks were higher in stress groups than in control group, indicating a more dynamic and active community after stress [22, 23] (Additional file 2: Table S6).

To delve deeper into the dynamic variations of microbial communities over time within the distinct treatment groups, 52 networks were established covering the entire temporal spectrum of the four treatments. Based on the network properties, the rhizosphere co-occurrence networks of different treatments followed distinct trajectories of change (Fig. 3D and Additional file 1: Fig. S8). The variations of network topological parameters were regressed against treatment time (Additional file 1: Fig. S9). The results showed a significant decrease in the total number of nodes (network size) with the progression of treatment time in both the salt stress and drought stress treatment groups, as well as in the total number of links and average degree (Fig. 3E and Additional file 1: Fig. S9). This suggested that the complexity of microbial networks in the salt stress and drought stress treatment groups continued to decrease, with the associations between microbes tending to simplify as the severity of stress intensified. The slope of network properties over time of the disease group was not statistically different in contrast to the two groups of abiotic stress. Overall, while the temporal network complexity of the three stress groups did not increase over time, their total networks were consistently more complex than those of the control group, indicating the rhizosphere microbial community of the stress groups with higher turnover rates and the recruitment of additional new members.

By simulating species extinction, we calculated the robustness (the resistance to node loss) of the overall networks under four treatments to investigate the impact of different treatment conditions on the stability of co-occurrence networks in the rhizosphere microbial community. Based on a random loss of species (where 50% of taxa were randomly removed), it was concluded that the robustness of stress networks was significantly higher than that of the control network [24] (Fig. 3F). In addition, the network vulnerability (the maximum decrease in network efficiency when a single node is deleted from the network) was highest in the control network [25] (Fig. 3G). To assess the importance of core and specific ASVs in the rhizosphere microbiome co-occurrence network, we quantified the impact of selectively removing core and specific ASVs on network robustness. The results showed that removing the core ASVs led to lower network robustness compared to the removal of a greater quantity of specific ASVs (Fig. 3F), underscoring the pivotal influence of the core ASVs on the network stability.

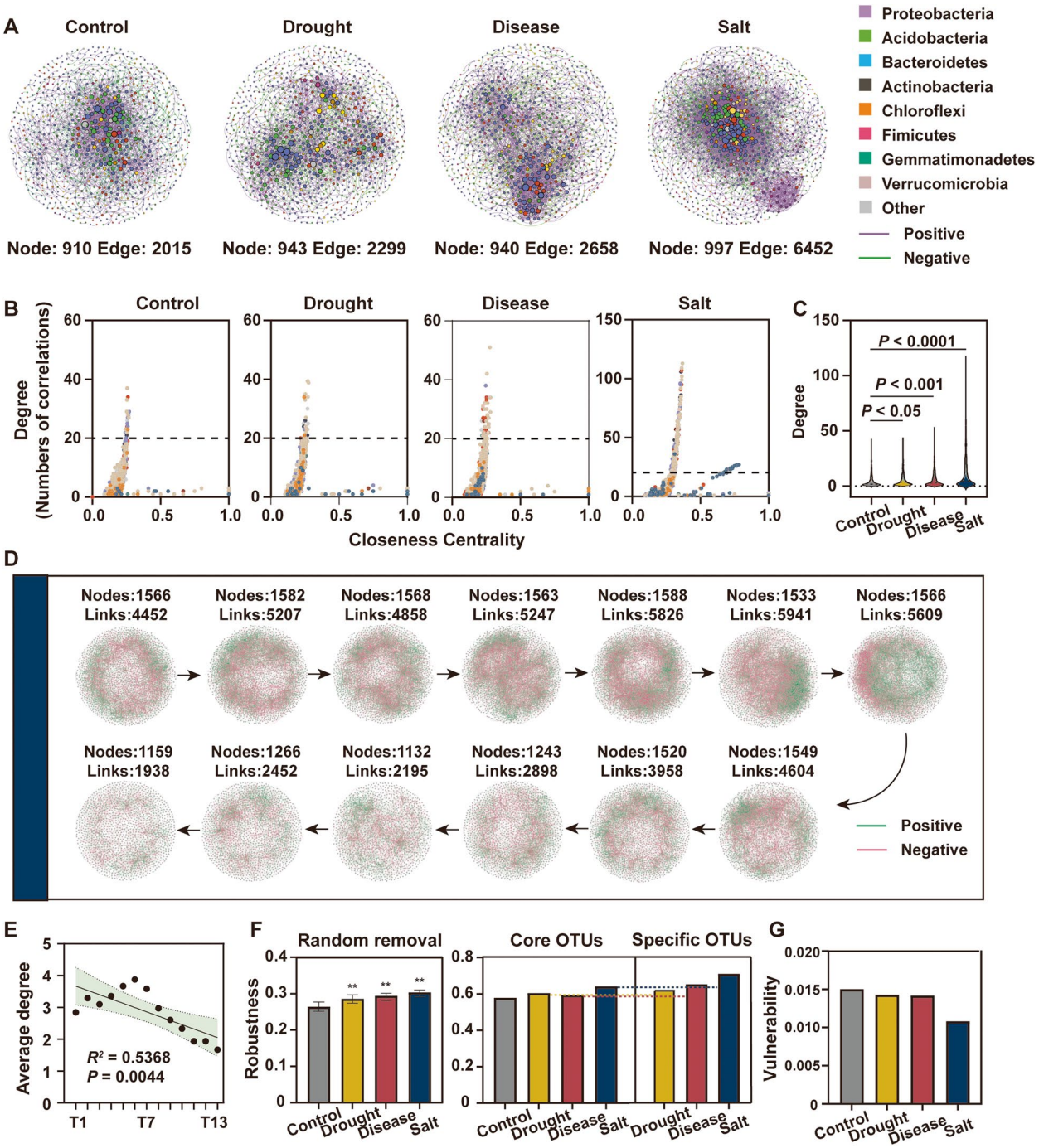

Fig. 3 Distinct co-occurrence networks of four treatments. **A** The overall co-occurrence networks of four treatments. The nodes are colored according to bacterial phylum. Node size indicates the degree of connection. Edge color represents positive (purple) and negative (green) correlations. **B** The distribution of the degree and closeness centrality for ASVs. **C** The degree of ASVs in different networks. The significance of difference was determined by nonparametric Kruskal–Wallis test . **D** The co-occurrence networks of salt treatment at 13 time points. **E** Temporal changes of average degree under salt stress treatment. R *2* represents the goodness of fit of a power-law model. **F** The robustness changes of random removal, the core ASVs removal, and the specific ASVs removal. **G** Network vulnerability measured by maximum node vulnerability in four networks.

Further eliminating the influence of varying ASVs numbers, we randomly sampled the same number of ASVs, core ASVs, and specific ASVs from the overall network. The significantly lower cumulative degree ranking of core ASVs compared to specific and random ASVs highlighted the closer interconnections and pivotal roles played by core ASV members within the network (Additional file 2: Table S7). Collectively, the preceding results indicated the potential stabilizing role for core ASVs under environmental variations, while specific ASVs contributed varying proportions of importance within particular environments.

Community assembly in different sub-communities

The neutral community model (NCM) was used to effectively estimate partial relationships between the occurrence frequency of ASVs and relative abundance changes (Fig. 4A). The results revealed that stress treatments reduced community stochastic assembly to varying extents, with the lowest variance observed in the salt treatment group at 25.1%, followed by the drought group (40.9%) and the disease group (48.3%). Moreover, we employed a null model to delineate the mechanisms of assembly processes, uncovering both deterministic ($|\beta NTI| \geq 2$) and stochastic processes ($|\beta NTI| < 2$) driving community assemblies (Fig. 4B). Following further analysis of microbial community structural changes between control and stress-treated groups, βNTI values primarily distributed within the < -2 interval among the three sample pairs, indicating that the shifts in microbial community structure following stress imposition were primarily driven by deterministic factors.

To dissect the ecological assembly processes of communities under diverse stresses, we narrowed our focus to examine the ecological patterns and assembly processes of specific sub-communities. Notably, the core sub-community exhibited the anticipated high ecological niche width, while the stress-specific microbial sub-communities demonstrated elevated niche width (Fig. 4C). RC-bray and βNTI were combined to identify the determinism and stochasticity of sub-community assembly. The differences in βNTI between the core microbial community and stress sub-communities were significantly observed (Fig. 4D). The core sub-community was mainly driven by homogenizing dispersal (39.7%) and undominated processes (47.6%) (Fig. 4E). The salt-specific and the drought-specific sub-communities were significantly affected by heterogeneous selection (88.4%; 73.7%), while the disease-specific sub-community was dominated by heterogeneous selection (56.2%) and undominated processes (29.5%).

Metagenomic data provide deeper insights into microbial interactions

To determine the role of shifts in the composition of rhizosphere microbial communities from the functional perspective, we performed metagenomic sequencing on samples from all treatments. The combined datasets of 48 rhizosphere samples contained a total of 591.96 Gbp of raw reads (Additional file 2: Table S8). Of 8.43 million genes in our dataset, we obtained approximately 28% functional annotations of the unigenes (2.34 of 8.43 million) and assigned 8858 KOs to the annotated unigenes (Fig. 5A, B).

Upon pairwise comparisons between stressed and control samples, the shared enrichment pathways under three stresses mainly involved in nutrient acquisition, secondary metabolism regulation, and environmental adaptation (Fig. 5C). Specifically, these shared KOs involved tyrosine metabolism (*maiA*), glycine, serine, and threonine metabolism (*ectA*), terpenoid and polyketide metabolism (*snoaL2*, *asm12*), fatty acid degradation (*gcdH*), and phosphate transport (*ugpA*) ($P < 0.05$, | ReporterScore |> 1.64, Additional file 2: Table S9). In addition, over-represented transcription factor families such as TetR/AcrR, NarL, and OmpR [26–29] are typically involved in metabolism, transport, and stress responses, processes that might be expected to be crucial under stress conditions in the rhizosphere ($P < 0.05$, | ReporterScore |> 1.64). These shared pathways likely contribute to broad-spectrum stress resistance, enhancing the ability of organisms to withstand multiple types of environmental stresses in natural settings.

Notably, each type of stress elicited distinct microbiome responses characterized by specific pathway enrichments. The disease group showed enrichment

(See figure on next page.)

Fig. 4 Assembly process structuring the bacterial community. **A** Fit of the neutral community model (NCM) of community assembly. The solid grey lines represent the best fit to the neutral community model, and the dashed grey lines indicate 95% confidence intervals around the model prediction. ASVs that occur more or less frequently than predicted by neutral community model are shown by red and blue, respectively. R *2* represents the fit to the model. **B** Difference of βNTI between four treatment communities. **C** The niche breadth of the core and specific ASVs groups. **D** Difference of βNTI between the core and specific ASVs groups. **E** The relatively explained ecological process of the core and specific communities based on the values of two indices, βNTI and RCbray. Un: undominated processed; DiL: dispersal limitation; HoD: homogenizing dispersal; HeS: heterogene selection.

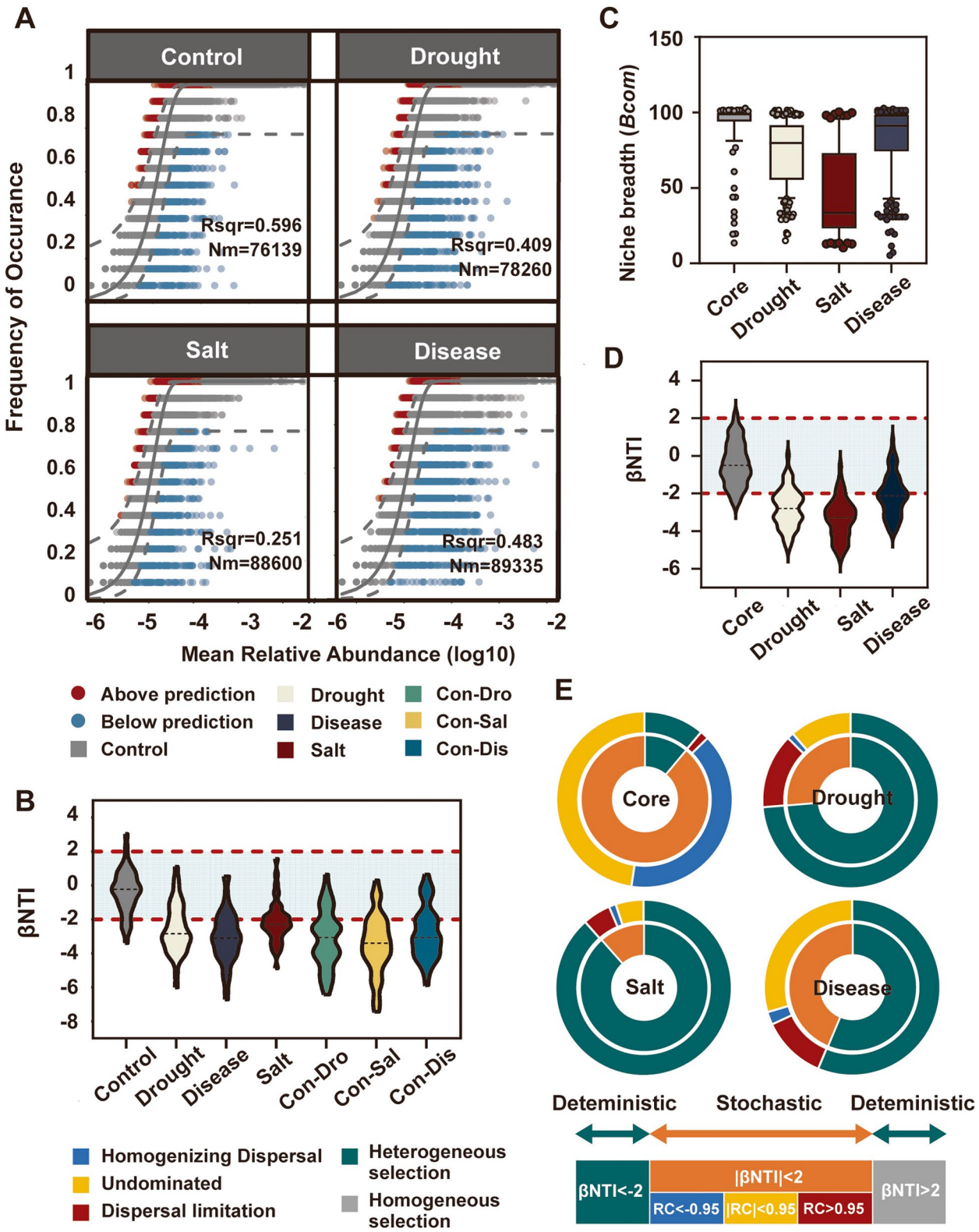

Fig. 4 (See legend on previous page.)

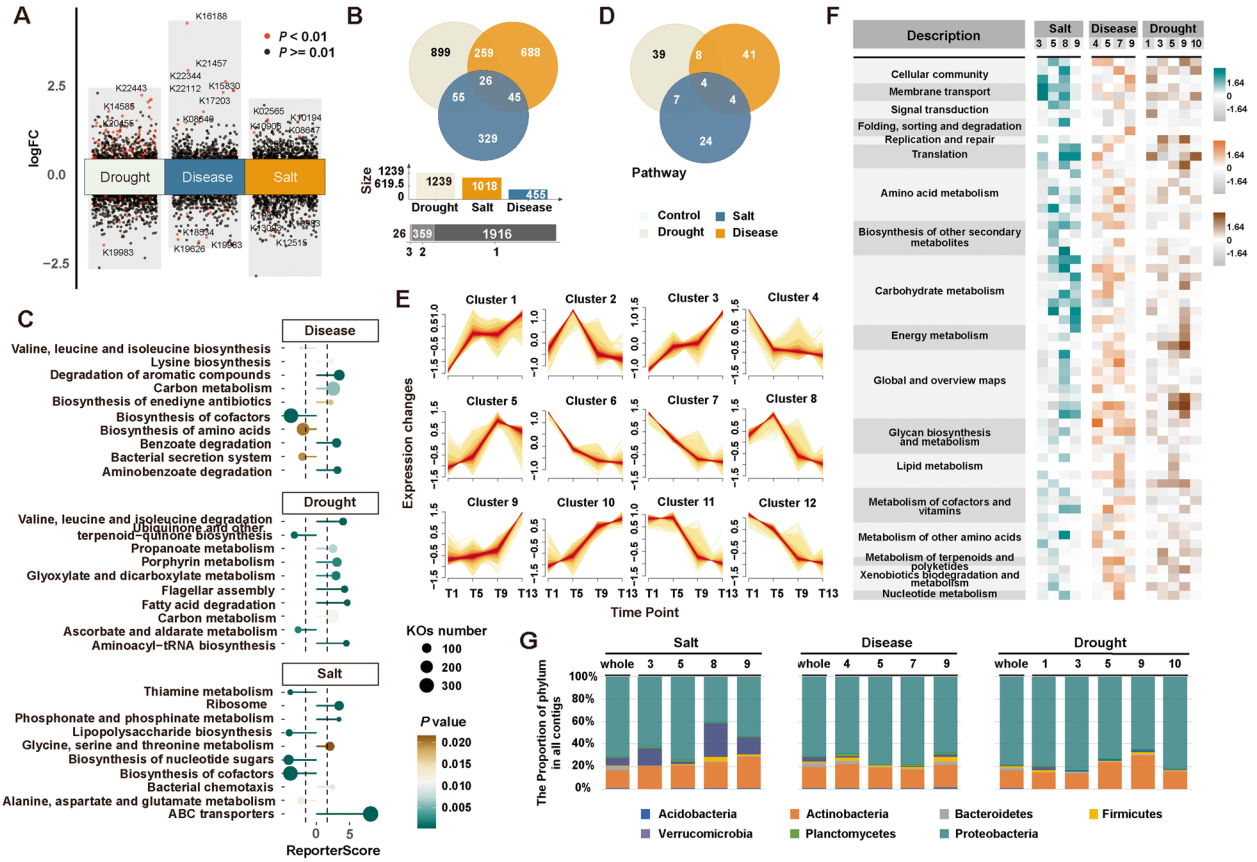

Fig. 5 Functional characteristics of bacterial communities under stresses. **A** Enrichment and depletion of the KOs, fold change > 2 or < − 2, respectively. **B** Venn diagram of enriched KOs in the salt, drought, and disease treatment groups. **C** The functional enrichment for salt, drought, and disease groups. **D** Venn diagram of enriched pathways in the salt, drought, and disease treatment groups. **E** Dynamics of gene expression during drought stress. Fuzzy c-means clustering grouped the expression profiles of gene expression atlas into 12 clusters. The x axis depicts drought samples from four key stages. **F** The functional enrichment for clusters with continuous upregulation. **G** Distribution of phylum for clusters with continuous upregulation.

in KOs associated with aromatic compound degradation and enediyne antibiotics biosynthesis. The coexistence of plant-released aromatic compounds for pathogen resistance and microbially produced enediyne antibiotics, known for their potent antibacterial properties, illustrated the complex defense strategies formed in the rhizosphere environment by the combined action of plants and microbes. Furthermore, genes encoding MCPs, flagellar proteins and a series of chemotaxis proteins (*MotA*, *MotD*, *CheZ*, *CheV*) were found to be upregulated in the salt and drought treatments (Additional file 2: Table S10). Consistent with previous research, we observed significant enrichment of cellular motility pathways (bacterial chemotaxis, flagellar assembly) in the rhizosphere soil under two abiotic stresses, which demonstrated that salt and drought stresses shaped the rhizosphere community dominated by the higher expression of bacteria involved in cell motility [30]. We also identified the significant enrichment of the ABC transporters pathway in the rhizosphere soil under salt stress. ABC transporter proteins are indispensable for bacterial adaptation to high salinity by reducing energy consumption, enhancing molecular absorption, and regulating osmotic pressure [31]. Overall, these results suggest that the rhizosphere microbiome shows a unique response to each treatment (Fig. 5D).

To further elucidate patterns of synergistic stress resistance among rhizosphere microbes, we classified all annotated genes into 12 clusters for each treatment based on their patterns of accumulation using the fuzzy c-means clustering algorithm [32, 33] (Fig. 5E and Additional file 1: Fig. S10). We specifically focused on clusters such as Cluster Sa3, Sa5, Sa8, and Sa9, which showed successive upregulation at four key time points. Functional enrichment results revealed that clusters exhibiting sustained upregulation under various stress conditions displayed diverse and clear enrichment patterns with specific emphases (Fig. 5F). For instance, genes involved

in biofilm formation, quorum sensing, and ABC transporters, were mainly enriched in Cluster Sa3. It suggested that the microbes within cluster Sa3 were actively involved in environmental adaptation and the preservation of internal and external environmental stability in salt-stressed poplar trees through multiple mechanisms. By contrast, genes involved in genetic information metabolic pathways, such as citrate cycle (TCA cycle) and oxidative phosphorylation, were enriched in Cluster Sa9. Remarkably, the clusters with relatively robust functions (Cluster Sa8, Di7, Dr9) exhibit a phylum distribution preference similar to that of specific ASVs groups identified in prior analyses, compared to the overall contigs distribution, potentially highlighting the essential roles these stress-specific species play in long-term stress resistance and adaptation (Fig. 5G). All together, these data suggest that microbes within different clusters may synergistically mitigate stress through diverse mechanisms, exhibiting distinct functional characteristics in the rhizosphere environment and appearing to be associated with stress-specific microbial communities.

Construction of synthetic communities and inoculation experiments

To evaluate the effects of the recruited bacteria on plant, we isolated 781 bacteria strains from the rhizosphere of four treatments by applying a culture-dependent approach using different cultivation media. Among them, 81 bacterial strains were identified belonging to core or stress-specific ASVs groups (Additional file 2: Table S11). According to their ability of dissolving inorganic P, solubilizing K, producing siderophile, producing IAA, and antagonistic activity, 15 strains were selected and inoculated separately into the sterile rhizosphere of plants to test whether they triggered plant growth promotion (Additional file 1: Fig. S11 A and Additional file2: Table S12). Plants inoculated with 14 strains exhibited significantly greater biomass and height compared to the control group, showing that 14 strains individually triggered increased plant growth promotion ($P < 0.01$) (Additional file 1: Fig. S11B and Additional file 1: Fig. S12).

Next, we selected a total of 9 bacterial strains to construct synthetic communities based on the fact that each core and stress-specific microbial groups contained at least 3 strains, aiming to achieve enhanced growth-promoting effects (Additional file 2: Table S13). It included species of the genera or family *Actinomyces*, *Kribbella*, and *Streptomyces* (phylum Actinobacteria), *Bacillus*, *Peribacillus*, and *Priestia* (phylum Firmicutes), and *Brucella*, *Vaeiovorax*, and *Sphingomondace* (phylum Proteobacteria) (Additional file 2: Table S13). Ultimately, six synthetic communities were constructed based on the division into different subgroups, including SCA (Drought + Core), SCB (Salt + Core), SCC (Disease + Core), SCD (Core), SCE (Drought + Disease + Salt), and SCF (All).

After 2 weeks of growth, plants treated with the six synthetic communities showed greater biomass and height compared to uninoculated plants. Among these, three synthetic communities composed of stress-specific groups along with the core group exhibited higher biomass and height compared to other three communities. Interestingly, the synthetic community containing all strains did not show improved performance (Additional file 1: Fig. S11 C).

To further investigate the effectiveness of synthetic communities in enhancing stress tolerance, particularly whether communities containing stress-specific groups exhibit superior effectiveness, we inoculated plants exposed to three stresses with six synthetic communities. To ensure the validity of the experimental results, we conducted the same experiment on 1-month-old and 3-month-old poplar trees and finally obtained similar results. As expected, synthetic communities containing stress-specific group performed better under specific stress condition (reflected in mortality rate, fresh weight, etc.) (Fig. 6A, Additional file2: Table S14). In addition, SCF-treated plants, which displayed lower biomass and plant height under normal growth conditions, unexpectedly demonstrated a 53.3% and 43.4% increase in height under two abiotic stress conditions. This phenomenon may be attributed to specific bacterial strains adapting alternative functionalities under stress conditions, thereby inducing responses in other microbial strains [34]. We selected stress-related marker genes from existing literature for transcriptional analysis to rule out the possibility that the increase in plant biomass was due to a general growth response (Fig. 6B). The SCA (*FUS3* [35] and *C3H35* [36]), SCB (*GRF15* [37] and *WOX11/12a* [38]), and SCC (*WRKY18* [39] and *TGA1* [40]) inoculation groups corresponding to drought, salt, and disease respectively showed the most significant upregulation of related resistance genes under stress. It was notable that the SCC-inoculation group containing core microbiota showed only a significant upregulation of *GRF15* expression. Taken together, these results highlight the importance of stress-specific microbes in responding to stress conditions.

Discussion

Here, we conducted a comprehensive analysis of amplicons and metagenomes from poplar across continuous time points under three different stress conditions and normal growth. This study showed that stresses induce a high degree of microbial dynamism within the poplar rhizosphere, with different types of stress leading to distinct variation patterns and shaping diverse microbial

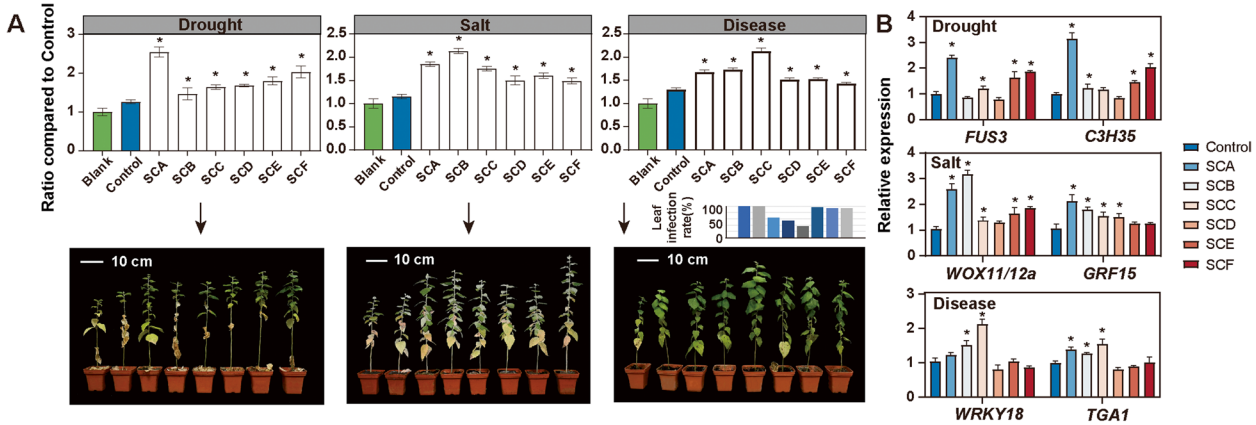

Fig. 6 The SynComs assist plants in coping with stress. **A** Ratio of the fresh weight of plants treated with SynComs to the blank group under stressed conditions. Under each column chart are corresponding pictures of the plants. Disease severity information (leaf infection rate) was also added to the disease treatment group. **B** Relative expression of stress-related genes to Actin in the poplar plants. Asterisks denote significant differences ($P < 0.01$).

communities. Microbial communities exhibit complex dynamics, with distinct species having fitness advantages under different sets of conditions determined by the surrounding biotic and abiotic environments [41]. Utilizing a random forest model, we delineated biomarker categories pertinent to various stress types and identified Actinobacteria (Actinobacteria), Alphaproteobacteria (Proteobacteria), and Clostridia (Firmicutes) as the most critical features, demonstrating their substantial correlation with stress. We were also able to use these models to accurately predict the types of stress experienced by plants in preprocessed data, despite the fact that these models were not trained on such data. This model proves essential for elucidating the relationships between specific taxonomic groups and stress types, and for deriving potential ecological implications.

The network analysis of co-occurrence patterns among taxonomic units facilitates the exploration of microbial interactions within complex communities, offering new insights into the structure of poplar rhizosphere microbiota under three types of stress conditions and normal growth. Microbial interactions shape microbial diversity and functionality, while changes in ecological network structure can impact ecosystem function and stability [25, 42, 43]. In this study, we found support for stresses disrupting microbial community networks: networks in stressed environments were larger and more complex, showcasing a more active microbial community compared to those in normal habitats. In contrast to the stressed groups, the control networks remained relatively static and simple over time, potentially indicating a more inactive or dormant state of the bacteria [44]. Both from the overall network perspective and when observing network trends at different time points, the microbial community networks in environments subjected to abiotic and biotic stress exhibited distinct pattern differences. Specifically, the network size, complexity, and stability of both types of abiotic stress decreased with increasing stress duration. Combining these findings with previous research, we conclude that microbes tend to reduce their associations under high environmental stress and be partially replaced by competitive species [45–48]. In contrast, networks under biotic stress showed a different trend, with no significant statistical differences in their subnetwork characteristics. We hypothesize that this foliar biotic stress does not sharply eliminate certain soil microbes but instead "gently" recruits new members [49–51]. Studies on tomatoes [52], Arabidopsis thaliana [53], and peppers [54] have shown that infection by above-ground pathogens can systematically send signals to the root system, thereby altering the rhizosphere microbial community by changing the plant's secretion pattern. Notably, our study reveals microbial community structures under different stresses, which helps delve into microbial interactions under various stress conditions.

Metagenomic analyses indicated that microbiome functional genes involved in nutrient acquisition, secondary metabolism regulation, and environmental adaptation were enriched in stressed plants compared to those normally growing. To be specific, these shared KOs were implicated in tyrosine metabolism, glycine, serine, and threonine metabolism, terpenoid and polyketide metabolism, fatty acid degradation, phosphate transport, and other metabolic and transport processes. We propose that this represents a broad-spectrum adaptive response to stress, illustrating that a coadaptive strategy exists for microbes and plants [55]. Generally, biotic and abiotic stresses are seldom compared together. However,

previous research has proposed that plants under stress conditions can balance microbe-mediated nutrient acquisition and defense. For instance, Arabidopsis's Phosphate Starvation Response 1 (PHR1), which modulates phosphate stress responses, also directly controls a set of functionally related plant immune system genes and contributes to the assembly of root microbiome, thereby integrating plant nutrient responses, immune functions, and microbiome assembly [56]. Increasing evidence suggested that there are interactions between different signaling pathways in plants, potentially by influencing the rhizosphere microbiome to cope with various types of stress encountered under field conditions [57, 58]. Exploring the functional overlap of microbiomes provides new insights into how microbial responses intersect under various stresses, which helps them act simultaneously and coordinately to maximize resource utilization. Microbiome breeding has become a transformative technology by controlling the composition and function of plant-associated microbial communities to achieve enhanced tolerance, improved nutrient uptake, or increased productivity [59, 60]. Specific functional genes play a crucial role in this process. For instance, specific M gene haplotypes can significantly enrich specific microbiome components and enhance protection against pathogens [61]; genes involved in the biosynthesis or regulation of plant metabolites, such as different lignin precursors and coumarins, can affect the plant microbiome, and optimizing the production of these compounds through targeted plant breeding is expected to reduce the global use of chemical pesticides and fertilizers [62, 63].

Plants not only utilize environment-derived microbiomes to regulate nutrient responses and immune systems but also attract beneficial microbes from the environment to cope with specific stresses, a strategy known as the "cry for help" [64]. Various stressors trigger unique responses, leading to diverse acclimatization and defensive strategies. In diseased microbiomes, enrichment of pathways involved in the degradation of aromatic compounds and enediyne antibiotics biosynthesis has been observed, underscoring the complex defensive strategies between plants and microbes. In response to pathogen attacks, stress can regulate the root exudate profile—through transport, biosynthesis, and secretion processes—to attract specific beneficial bacteria that aid in defense [65]. Subsequently, these beneficial microbes employ antimicrobial compounds and quorum-sensing quenching molecules to inhibit pathogen growth and virulence [66, 67]. Furthermore, both salt and drought, as abiotic stresses, initially alter soil properties to rapidly eliminate a subset of unsuitable microbes and modify the root exudate secretion profile to trigger a "cry for help." Consistent with our results, previous studies have confirmed that salt stress enhances the secretion of xanthine by plants, which enriches plant growth-promoting *Pseudomonas* by stimulating its motility [30]. Clustering analysis of annotated genes identified distinct and clear enrichment patterns under three stress conditions, aiding in the classification of microbes involved in the same biological processes and highlighting the interactions among coexisting microbes. This result will facilitate the more precise identification of functional microbes and the development of functional synthetic communities in the future.

Given the presence of multiple treatment groups, our focus was on examining the core microbiota and stress-specific microbes to assess their contributions under stress conditions. The minimal overlap between core and stress-specific microbiota underscores their distinct ecological roles. Core taxa, which persist across treatments, likely provide constitutive functions essential for host health, such as nutrient acquisition and immune priming [68]. In contrast, stress-specific microbes may act as facultative mutualists, recruited to address acute environmental challenges. This segregation aligns with the "ecological filter" theory, where host selection and environmental stressors shape microbiota assembly [69]. The low overlap suggests minimal functional redundancy between core and stress-adaptive communities, which could reflect niche partitioning to avoid competition. Alternatively, it may indicate rapid microbial adaptation to stressors via horizontal gene transfer or community succession, as observed in rhizosphere studies [70]. Combined with the co-occurrence network and ecological indicators analysis, we found that the removal of core microbiota had the most significant impact on network stability and the core microbiota exhibited a broader niche width, implying their crucial role in maintaining community structure stability. This finding aligns with studies demonstrating the ecological importance of core microbiota in preserving functional stability in reforestation ecosystems [6]. While stress-specific microbes were essential for maintaining the structure of the co-occurrence network within their respective stress environments, their impact was less pronounced compared to core microbiota. Further analysis using null and neutral models revealed that the assembly of stress-specific microbiota is primarily driven by deterministic processes, whereas the assembly of core microbiota is governed by stochastic processes. Generally, the core microbiome identified by the definition method of membership comprised the abundant taxa common in the host [71]. Many studies on the community assembly of abundant taxa, such as those conducted in wetland soils [72], contaminated soils [73], and loess plateau soils [74], have similarly demonstrated that stochastic processes governed

the assembly of abundant taxa. Core communities with broader niche widths are considered more versatile in metabolic functions and better able to withstand environmental fluctuations [75, 76]. It has been shown that stochastic processes lead to higher diversity and transition rates [77], suggesting that the core taxa dominated by stochastic processes are more responsible for maintaining community and functional stability. Since deterministically assembled communities exhibited enhanced functionality compared to those assembled stochastically [78], it is likely that stress-specific microbiota contributes more to the function of the ecosystem in particular environments. Within low-diversity extreme environments, bacteria with "specialized functions" play important roles in the ecosystem that reduce environmental stress and increase the survival probability of other microbes lacking such functions [79]. Core microbiota and stress-specific microbiota simultaneously facilitated species interactions through different mechanisms, and the trade-off between them affects the community's potential to acclimatize to new environments. Although the roles and correlations of these microbiota have been proposed, the protective mechanisms and functional contributions of these core and stress-specific microbial communities still require separate and collective verification using cultivation-based approaches.

Based on the above conclusions, we conducted bacterial separation and selected strains based on the classification of core and stress-specific groups to further construct synthetic communities. Leveraging the observable key characteristics of the strains and recent advancements in microbiome research, we endeavored to select isolatable rhizosphere bacterial strains that are representative of the four groups to construct the synthetic community. Among them, bacterial strains from the genera or families Actinomyces, Kribbella, and Streptomyces (phylum Actinobacteria), Bacillus, Peribacillus, and Priestia (phylum Firmicutes), and Brucella, Variovorax, and Sphingomonas (phylum Proteobacteria) have been shown to promote plant growth. By employing the strategy of concurrently applying both core and specific groups, we observed significant improvements in plant performance under both normal and stress conditions. The measurement of the transcription of the stress-related genes for the three types of stresses further confirmed that the microbial community not only promoted plant growth, but indeed initiated the stress resistance processes of plants, such as ROS scavenging (*WOX11/12a*), regulating plant hormone signals like ABA (*FUS3*), and activating immune responses (*WRKY18*, *TGA1*). Notably, inoculation with either core or specific groups alone did not yield substantial enhancements in plant stress tolerance, demonstrating the indispensable role of these microbiota in the rhizosphere environment [13, 80]. The core microbiota was likely to merely tend to trigger the general plant growth promotion effect. However, the synthetic community containing all strains exhibited poor performance under normal growth conditions, which may be attributed to functional redundancy among these species, as they perform similar roles within the given community [81–83]. A possible explanation for the highest plant height observed in the SCF-inoculated groups under two types of abiotic stress is that functional redundancy among species may be altered due to shifts in their functional roles within the modified environmental conditions [34, 84]. Species that are redundant under normal growth conditions may turn out to be essential performers or partners in new interspecific interactions after environmental change [34]. It is undeniable that the current seven synthetic communities cannot fully possess all bacterial interactions and functions within the four groups. However, given the unquestionable difficulty in isolating these specific microbes, future research might attempt innovative approaches such as microfluidic cultivation, membrane diffusion-based cultivation, and cell sorting-based cultivation to construct more comprehensive core and stress-specific communities [85, 86].

Conclusions

Overall, our research demonstrated the alteration patterns and functional characteristics of the microbiome under different growth conditions. Meanwhile, it further indicated that the core microbiota and the stress-specific microbiota under stress each have their own functions and are both indispensable, jointly exerting beneficial effects on the poplar host. The core microbiota makes a prominent contribution in maintaining community stability and is biased towards promoting plant growth. While the stress-specific microbiota is recruited by plants and exhibits diverse protective potentials in the face of different stresses by regulating osmotic pressure, secreting antibiotics, and other means. This study provides new insights into the potential mechanisms by which the microbiome helps plants cope with stress and offers a theoretical basis for constructing an efficient plant–microbe stress resistance system.

Methods

Experimental design and sampling

To analyze the influence of three kinds of stress on rhizosphere microbial communities, 84 K poplars were planted in plastic house in in Baishan Town, Changping District, Beijing, China (40.14807° N, 116.35353° E).

The soil used in this study was collected from five sites in Beijing where poplar trees had been planted for more than 10 years. The topsoil (10–15 cm) was removed, and

the layer (15 − 30 cm) was collected. Then, all soils were sieved through a 0.5-cm mesh screen at room temperature to remove plant debris, mixed in equal proportions, and stored in the cold room (4℃) for further use. When the experiment commenced, we retrieved the soil from the cold room maintained at 4 °C, allowed it to reach room temperature, and then mixed it with the sterile soil in equal proportion to ensure an adequate nutrient supply for plant growth. The sterile soil used in this study was obtained by thoroughly mixing vermiculite, perlite, and moss peat in 1:1:2 volumes, and then sterilizing it in the autoclave at 121 °C for 20 min twice at 24-h intervals.

A semi-open mesocosm system was used in this paper, guaranteeing repeated collection of rhizosphere soil from each individual plant without damaging the root system, which consisted of an inner reticular container and several outer reticular containers [87]. All containers were filled with previously prepared soil with microbes. The inner container (root compartment) was made of the 150-μm nylon mesh net with a height of 20 cm and a diameter of 6 cm, which allowed microbes to pass freely and prevented the root from spreading and growing at will. The outer container (rhizosphere soil compartment) was the rectangular 150-μm nylon mesh bag with a height of 20 cm and a width of 2 cm. Eight outer containers were evenly arranged around the inner container, with no gap left in the middle. The method of obtaining rhizosphere soil in this way has been verified by preliminary experiments. Each rectangular mesh bag could be removed individually during sampling according to the experimental design. Seven groups of semi-open mesocosm systems were evenly spaced separately in twelve planting tanks with a length of 2.8 m and a width of 0.4 m that were filled with microbial soil.

Plants were grown in the plastic house from Mar. 30 to Oct. 25, 2021. In the tissue culture room of the laboratory, 200 bottles of tissue culture seedlings with the same growth and the same propagation time, growing to about 8 cm, were selected. The roots of the tissue culture seedlings were cleaned, dipped in carbendazim and nutrient solution, and then put in pots containing sterile soil in the greenhouse respectively. Then the seedlings were hardened for a month to acclimatize to the greenhouse environment. Until April 30, 182 healthy seedlings were counted as living. Afterwards, strong seedlings growing to about 15 cm were selected, and they were planted in the interior container of the semi-open ecosystem after gently removing the soil with sterile water. The entire semi-open ecosystem was placed in the planting tank and covered with about 2 cm of soil.

The plants were grown under normal conditions in this apparatus for 3 months with twice-weekly irrigation. Plant treatments were initiated on July 30 th, 2021. After conducting comprehensive pre-experiments, we determined that the 200 mmol/L NaCl solution and 10% PEG6000 solution, which were the closest to the semi-lethal dose, would serve as the final experimental concentrations for salt and drought stress induction respectively. To induce salt stress, a quarter of the 12 planting tanks were irrigated twice a week with a NaCl solution at a concentration of 200 mmol/L. For drought stress treatment, three planting tanks were irrigated twice a week with a 10% PEG6000 solution, while three other planting tanks were inoculated with 100 μL of *Colletotrichum gloeosporioides* BJ12 [88] conidial suspension (1×10^6 spores/mL) on their third and fifth leaves. Through preliminary experiments, we have confirmed that the onset time of BJ12 is between 5 and 7 days. Therefore, we initiated the treatment 1 week in advance and ensured at all times that two leaves of each plant were infected, with timely re-inoculation whenever necessary. The remaining three planting tanks served as the control group and received normal watering twice a week, like the plants in the group that were infected with pathogens. To eliminate the influence of external factors such as geographical location, the three treatments and the control were arranged in an alternating pattern in the 12 planting tanks.

Soil sampling was performed once a week. Each time, a nylon mesh bag containing the rhizosphere soil of all plants was randomly selected, and the soil outside each semi-open mesocosm was excavated. These were respectively mixed uniformly in accordance with the planting tanks as rhizosphere samples and field soil samples. The soil in each planting tank was regarded as one replicate of this treatment, with a total of three replicates. The amplicons were submitted for testing once a week, and the metagenomes were sent for testing once every 2 weeks. Meanwhile, the plant height, leaf size, leaf number, ground diameter, and photosynthetic indicators of the plants were measured on a weekly basis.

DNA extraction and Illumina sequencing

Total DNA was extracted from 0.5 g of rhizosphere or soil samples using DNeasy PowerSoil Pro Kits (Qiagen, Germany) in accordance with the manufacturer's protocol. The DNA concentration and purity were assessed on a 1% agarose gel, and subsequently, sterile water was used to dilute the DNA to a final concentration of 1 μg/μL based on the initial measurement. The PCR product targeting the V4 region of bacterial 16S rRNA gene was amplified using specific primers 515 F: GTGYCA GCMGCCGCGGTAA and 806R: GGACTACNVGGG TWTCTAAT [47]. The reaction mixture consisted of 15 μL of Phusion® High-Fidelity PCR Master Mix (New England Biolabs), 0.2 μM of forward and reverse primers, and 10 ng of template DNA. The thermal cycling

conditions were as follows: initial denaturation at 98 °C for 1 min, followed by 30 cycles of denaturation at 98 °C for 10 s, annealing at 50 °C for 30 s, extension at 72 °C for 30 s, and a final extension step at 72 °C for 5 min. The PCR products were quantified, thoroughly mixed in equidensity ratios, and subsequently purified using the Qiagen Gel Extraction Kit (Qiagen, Germany). Finally, the library was sequenced on the Illumina NovaSeq platform and 250 bp paired-end reads were generated.

For metagenomic library preparation, the metagenomic DNA was randomly fragmented by the Covaris ultrasonic disruptor. Subsequently, the entire process of library preparation was accomplished through sequential steps including end repair, addition of A tails, addition of sequencing adapters, purification, and PCR amplification. After quality control, quantification and normalization of the DNA libraries, reads were generated from the Illumina HiSeq6000 platform according to the manufacturer's instructions.

Amplicon data analysis

The paired-end reads were merged into a single sequence using USEARCH v11.0. 667. We employed the fastq_maxee_rate option to remove the low-quality reads with the error rate exceeding 1%. And then, reads shorter than 100 bp were discarded through the fastq_minlen option of VSEARCH 2.21.1. Biological reads were identified with 100% sequence similarity to generate the ASV table through the unoise3 option [89] of USEARCH. Taxonomic assignment was performed by comparing the sequences against the SILVA reference database for bacteria using QIIME v1.9.1.

For subsequent analysis, the table format results were converted to Biological Observation Matrix (BIOM) format using BIOM 2.1.5. We proceeded by utilizing multiple scripts within QIIME v1.9.0 to standardize and calculate both alpha and beta diversity metrics. Kruskal–Wallis test was carried out to compare the difference of alpha diversity. The principal coordinate analysis (PCoA) plots were generated from Bray–Curtis similarity matrices by using R package ggplot2. PERMANOVA was used to assess the effect of compartment (bulk soil or rhizosphere), time period (weeks 1–13), and treatment (control, drought, disease, or salt) on the bacterial community variation either detected by Bray–Curtis dissimilarities using the adonis command in vegan package in R. To identify the important predictor that was most sensitive to the stress types, the Random forest model was conducted using the "randomForest" R package. After 1000 iterations, features were ranked by importance based on model accuracy. The optimal number of biomarkers was determined via 5 repetitions of tenfold cross-validation. Random forest models were constructed for different taxonomic levels, and the best classification level was selected according to model performance metrics. The abundance-occupancy distribution was used to explore the frequency and quantity of microbes across different treatments and time series. After sorting the data based on occupancy, a weighted index was calculated. Subsequently, the contribution of ASVs to the Bray–Curtis similarity was computed.

Metagenomic data analysis

The raw reads obtained from metagenome sequencing were employed to generate clean reads through the removal of adaptor sequences, trimming, and elimination of low-quality reads. Then, further quality control and host removal were conducted through kneaddata v0.10.0. The pooled metagenomic reads from each group were de novo assembled using Megahit v1.0 with the default parameter. Gene annotation was performed using prokka v1.13.3, and a non-redundant gene set was constructed using CD-HIT-est with the identify cutoff of 95%. The meta option of the salmon software was selected for gene quantification to generate the gene abundance matrix. Diamond software was used to align the protein sequences against the KO database for functional gene annotation. The Reporter score algorithm was used to calculate the enrichment level of functional patterns. Fuzzy c-means (FCM) algorithms were employed for gene clustering, implemented using the Mfuzz package in R.

Network construction and analysis

The rhizosphere soil community networks of each treatment were constructed based on the relative abundance of ASVs using SparCC correlation to evaluate the complexity of the interactions in rhizosphere microbiota. The correlation matrix of random values was obtained from the original dataset through the bootstrap approach. Subsequently, by comparing the distribution of the values in the observed correlation matrix within that of the random value correlation matrix, pseudo p-values are generated. The correlation matrix and the p-value matrix are merged to obtain the ultimate network. The high relative abundances (> 0.01%) and statistically significant correlations ($P < 0.01$, Spearman's correlations with > 0.8 or < -0.8) among ASVs were included into the network analyses [90, 91]. A set of measures (i.e., the numbers of nodes and edges, average degree, average path length, clustering coefficients, network diameter, and modularity) were calculated to analyze the topology of the network. Based on linear regression analysis, the changing trends of the network topological properties with the variation of stress time were presented. Networks were

visualized and explored with the interactive platform Gephi (http://gephi.github.io/).

In order to verify the stability of rhizosphere microbial co-occurrence networks, species extinction was simulated through random species loss, and then the robustness and vulnerability of the network were assessed [25]. Robustness was defined as the proportion of remaining species in the network after random or targeted node removal. Vulnerability measured the relative contribution of specific nodes to global efficiency. Both robustness and vulnerability metrics were calculated using the ggClusterNet package, with the rand.remov.once function defined to simulate species extinction. And to further determine the importance of sub-communities to the stability of the overall community, we randomly removed the nodes belonging to the sub-communities in the network 100 times and generated 100 random networks [25]. Due to the different numbers of species in the sub-communities, we specified the same number (50) of nodes to be removed. For each randomization, a set of network topological properties was calculated, and finally the cumulative ranking and confidence interval of the characteristics were obtained.

Quantification of ecological modeling

To evaluate ecological studies of community structure and species co-occurrence, it is critical to quantify the degree of resource division (i.e., niche overlap). The value of Levin's niche breadth and niche overlap of the subcommunity was calculated in the R environment (http://www.r-project.org) using spaa. The average of B-values from all taxa within one subcommunity was calculated as the community-level B-value (Bcom). Similarly, the average of O-values from taxon pairs within the community was calculated as the community-level O-value (Ocom).

The null model and neutral community model were used to investigate the importance of deterministic and stochastic processes on the bacterial community assembly. The Raup–Crick index (RC-Bray) and β nearest-taxon index (βNTI) were combined to assess the mechanisms of community assembly. Bray–Curtis-based Raup-Crick (RCbray) is a metric of taxonomic β-diversity. $|\beta NTI| < 2$ indicates that community assembly is dominated by stochastic processes. $\beta NTI < -2$ indicates that community assembly is dominated by heterogeneous selection; $|\beta NTI| < 2$ and $RC < -0.95$ indicate that community assembly is dominated by homogenizing dispersal; $|\beta NTI| < 2$ and $|RC| < 0.95$ indicate that community assembly is dominated by undominated process; $|\beta NTI| < 2$ and $RC > 0.95$ indicate that community assembly is dominated by dispersal limitation; $\beta NTI > 2$ indicates that community assembly is dominated by homogeneous selection.

Bacterial isolation from the rhizosphere and inoculation of SynComs

The PBS washing solution was diluted, dispensed, and incubated in 1/10 TSB medium in 96-well microtiter plates at 28 ℃ for 14 days and was indexed using the two-sided barcode PCR system based on Illumina sequencing [86, 92]. The recovered bacteria were compared with the members of the corresponding rhizosphere microbiota with >99% 16S rRNA gene identity. Each ASV identified from the recovered bacteria was selectively cultured and purified on 1/2 TSA medium. The bacterial universal primers 341 F/1075R and 63 F/1389R were employed to amplify the 16S rRNA genes. Subsequently, the obtained sequences were subjected to BLAST searches against the NCBI database and the Ribosomal Database Project reference database for bacterial classification purposes. Moreover, the sequences of individual bacterial isolates were compared through BLAST with the sequences of ASV representatives derived from 16S rRNA sequences, and then assigned to the corresponding ASVs. In total, 81 strains were identified as belonging to core or stress-specific ASVs groups and were stored at −80 ℃ with 50% glycerin solutions. Try to select bacteria from different genera and choose multi-functional strains based on their abilities to solubilize phosphorus and potassium, produce siderophores, produce IAA, and exhibit antagonistic capabilities. The selected strains were inoculated on LB plates at 37 ℃ for 2 days. The appearance of strain colonies including size, shape, gloss, color, consistency, and transparency was observed. Pikovskaya (PKO) mediums, silicate bacteria mediums, and CAS detection medium (CAS) were used to test the phosphate-solubilizing and potassium-releasing capacity of the strain [93–95]. LB medium supplemented with L-tryptophan was used to measure the IAA production of the strain [96]. All strains were propagated in TSB medium using the shake–flask fermentation method with a culture period of 4 days at 25 °C. Each bacterial fermentation broth was centrifuged at 4000 ×*g* for 8 min, and then resuspended in PBS. To standardize the initial state of each strain, the OD_{600} values were systematically monitored throughout the resuspension process. The OD_{600} was adjusted to 0.2 (approximately 10^8 cells/mL). Ensure that the core and the three stress-specific groups each contain more than three ASVs. Subsequently, the strains were equimolarly mixed as SynComs. Finally, each plant received a cumulative total of approximately 10^9 cells [8]. To ensure the validity of the experiment, we had 6 biological replicates for each treatment, and conducted the same experiment on 1-month-old and 3-month-old poplar trees. Furthermore, a blank control group and a control group were established. In the blank control group, the plants were carefully excavated prior to inoculation and subsequently

placed in sterilized soil. During the inoculation process, an equal volume of PBS buffer was administered by irrigation. Similarly, in the control group, an equivalent volume of PBS buffer was applied via irrigation during inoculation.

Gene expression

The genes *FUS3* and *C3H35* have been shown to be related to drought resistance of poplar; *GRF15* and *WOX11/12a* have been confirmed to be associated with salt tolerance in poplar; *WRKY18* and *TGA1* have been confirmed to be related to disease resistance of poplar. *Actin* was chosen as an internal standard. Relative expression level (fold change) was calculated by the $2^{-\Delta\Delta Ct}$ method. For each sample, three biological replicates and four technical replicates were conducted respectively. All the primers used in RT-qPCR are listed in Additional file 2: Table S15.

Supplementary Information

The online version contains supplementary material available at https://doi.org/10.1186/s40168-025-02103-z.

Additional file 1: Supplementary Figures.

Additional file 2: Supplementary Tables.

Acknowledgements
We are particularly grateful to Dr Francis Martin from INRA-Université de Lorraine, France, for his invaluable support, insightful discussions, and constructive comments throughout the course of this research.

Authors' contributions
JBX and SJL conceived and designed the project; SJL, JDW, HFW, ZLJ and XZ collected the samples; SJL, JDW and ZC conducted the experiments; SJL and JDW analyzed the data; SJL wrote the draft manuscript; JBX and DQZ discussed and revised the manuscript. All authors read and approved the final manuscript.

Funding
This work was supported by funding from the Fundamental Research Funds for the National Key R&D Program of China (nos. 2023YFD2200203, 2022YFD2201600; and 2022YFD2200602), the Project of the National Natural Science Foundation of China (nos. 32371906 and 32022057), Forestry and Grassland Science and Technology Innovation Youth Top Talent Project of China (no. 2020132607). Central Universities [QNTD202305, BFUKF202413], the 111 Project (No. B20050).

Data availability
The raw amplicon data are publicly accessible in the Genome Sequence Archive of the Beijing Institute of Genomics BIG Data Center, Chinese Academy of Sciences, under CRA019448. The metagenome data could be accessed under CRA019435.

Declarations

Ethics approval and consent to participate
Not applicable.

Consent for publication
Not applicable.

Competing interests
The authors declare no competing interests.

Author details
[1]State Key Laboratory of Tree Genetics and Breeding, College of Biological Sciences and Technology, Beijing Forestry University, Beijing 100083, China. [2]National Engineering Research Center of Tree Breeding and Ecological Restoration, Beijing Forestry University, No. 35, Qinghua East Road, Beijing 100083, People's Republic of China. [3]The Tree and Ornamental Plant Breeding and Biotechnology Laboratory of National Forestry and Grassland Administration, Beijing Forestry University, Beijing, China.

Received: 4 November 2024 Accepted: 31 March 2025
Published online: 04 May 2025

References

1. Bulgarelli D, Garrido-Oter R, Münch Philipp C, Weiman A, Dröge J, Pan Y, McHardy Alice C, Schulze-Lefert P. Structure and Function of the Bacterial Root Microbiota in Wild and Domesticated Barley. Cell Host Microbe. 2015;17(3):392–403.
2. Chaparro JM, Badri DV, Vivanco JM. Rhizosphere microbiome assemblage is affected by plant development. ISME J. 2014;8(4):790–803.
3. Smith DL, Praslickova D, Ilangumaran G. Inter-organismal signaling and management of the phytomicrobiome. Front Plant Sci. 2015;6:722.
4. Custer GF, Gans M, Diepen LTAv, Dini-Andreote F, Buerkle CA. Comparative Analysis of Core Microbiome Assignments: Implications for Ecological Synthesis. mSystems 2023;8(1):e01066–01022.
5. Toju H, Peay KG, Yamamichi M, Narisawa K, Hiruma K, Naito K, Fukuda S, Ushio M, Nakaoka S, Onoda Y, et al. Core microbiomes for sustainable agroecosystems. Nature Plants. 2018;4(5):247–57.
6. Jiao S, Chen W, Wei G. Core microbiota drive functional stability of soil microbiome in reforestation ecosystems. Glob Change Biol. 2021;28(3):1038–47.
7. Li H, La S, Zhang X, Gao L, Tian Y. Salt-induced recruitment of specific root-associated bacterial consortium capable of enhancing plant adaptability to salt stress. ISME J. 2021;15(10):2865–82.
8. Schmitz L, Yan Z, Schneijderberg M, de Roij M, Pijnenburg R, Zheng Q, Franken C, Dechesne A, Trindade LM, van Velzen R, et al. Synthetic bacterial community derived from a desert rhizosphere confers salt stress resilience to tomato in the presence of a soil microbiome. ISME J. 2022;16(8):1907–20.
9. Kwak M-J, Kong HG, Choi K, Kwon S-K, Song JY, Lee J, Lee PA, Choi SY, Seo M, Lee HJ, et al. Rhizosphere microbiome structure alters to enable wilt resistance in tomato. Nat Biotechnol. 2018;36(11):1100–9.
10. Yin J, Gentine P, Slater L, Gu L, Pokhrel Y, Hanasaki N, Guo S, Xiong L, Schlenker W. Future socio-ecosystem productivity threatened by compound drought–heatwave events. Nat Sustain. 2023;6:259–72.
11. Julkowska MM, Testerink C. Tuning plant signaling and growth to survive salt. Trends in Plant Science. 2015:586–594.
12. Fernández-González AJ, Cardoni M, Cabanás CG-L, Valverde-Corredor A, Mercado-Blanco J. Linking belowground microbial network changes to different tolerance level towards Verticillium wilt of olive. Microbiome 2020;8(1):11.
13. Niu B, Paulson JN, Zheng X, Kolter R. Simplified and representative bacterial community of maize roots. Proc Natl Acad Sci. 2017;114(12):E2450–9.
14. Timm CM, Carter KR, Carrell AA, Jun SR, Weston DJ. Abiotic Stresses Shift Belowground Populus -Associated Bacteria Toward a Core Stress Microbiome. mSystems. 2018;3(1):e00070–00017.
15. Bulgarelli D, Schlaeppi K, Spaepen S, van Themaat EVL, Schulze-Lefert P. Structure and Functions of the Bacterial Microbiota of Plants. Annu Rev Plant Biol. 2013;64(1):807–38.
16. Zhang C, Heijden MVDVD, Dodds BK, Nguyen TB, Spooren J, Held A, Cosme M, Berendsen R. A tripartite bacterial-fungal-plant symbiosis in the mycorrhiza-shaped microbiome drives plant growth and mycorrhization. Microbiome. 2023;12:13.
17. Liu H, Li J, Singh BK. Harnessing co-evolutionary interactions between plants and Streptomycesto combat drought stress. Nature Plants. 2024;10(8):1159–71.

18. Leblanc N. Bacteria in the genus Streptomyces are effective biological control agents for management of fungal plant pathogens: a meta-analysis. Biocontrol. 2021;67:111–21.
19. Nakayasu M, Takamatsu K, Kanai K, Masuda S, Yamazaki S, Aoki Y, Shibata A, Suda W, Shirasu K, Yazaki K, et al. Tomato root-associated Sphingobium harbors genes for catabolizing toxic steroidal glycoalkaloids. mBio. 2023;14(5):e00599–00523.
20. Sarao SK, Boothe V, Das BK, Gonzalez-Hernandez JL, Brzel VS. Bradyrhizobium and the soybean rhizosphere: Species level bacterial population dynamics in established soybean fields, rhizosphere and nodules. Plant and Soil. 2025;508(1):515–30.
21. Romanowski SB, Lee S, Kunakom S, Paulo BS, Recchia MJJ, Liu DY, Cavanagh H, Linington RG, Eustáquio AS. Identification of the lipodepsipeptide selethramide encoded in a giant nonribosomal peptide synthetase from a Burkholderia bacterium. Proc Natl Acad Sci. 2023;120(42):e2304668120.
22. Guo B, Zhang L, Sun H, Gao M, Yu N, Zhang Q, Mou A, Liu Y. Microbial co-occurrence network topological properties link with reactor parameters and reveal importance of low-abundance genera. npj Biofilms and Microbiomes. 2022;8(1):3.
23. de Vries FT, Griffiths RI, Bailey M, Craig H, Girlanda M, Gweon HS, Hallin S, Kaisermann A, Keith AM, Kretzschmar M, et al. Soil bacterial networks are less stable under drought than fungal networks. Nat Commun. 2018;9(1):3033.
24. Montesinos-Navarro A, Hiraldo F, Tella JL, Blanco G. Network structure embracing mutualism–antagonism continuums increases community robustness. Nature Ecology & Evolution. 2017;1(11):1661–9.
25. Yuan MM, Guo X, Wu L, Zhang Y, Xiao N, Ning D, Shi Z, Zhou X, Wu L, Yang Y, et al. Climate warming enhances microbial network complexity and stability. Nat Clim Chang. 2021;11(4):343–8.
26. Schmidl SR, Ekness F, Sofjan K, Daeffler KNM, Brink KR, Landry BP, Gerhardt KP, Dyulgyarov N, Sheth RU, Tabor JJ. Rewiring bacterial two-component systems by modular DNA-binding domain swapping. Nat Chem Biol. 2019;15(7):690–8.
27. Ramos JL, Martínez-Bueno M, Molina-Henares AJ, Terán W, Watanabe K, Zhang X. Gallegos MaT, Brennan R, Tobes R. The TetR Family of Transcriptional Repressors. Microbiol Mol Biol Rev. 2005;69(2):326–56.
28. Zschiedrich CP, Keidel V, Szurmant H. Molecular Mechanisms of Two-Component Signal Transduction. J Mol Biol. 2016;428(19):3752–75.
29. Cuthbertson L, Nodwell JR. The TetR Family of Regulators. Microbiol Mol Biol Rev. 2013;77(3):440–75.
30. Zheng Y, Cao X, Zhou Y, Ma S, Wang Y, Li Z, Zhao D, Yang Y, Zhang H, Meng C, et al. Purines enrich root-associated Pseudomonas and improve wild soybean growth under salt stress. Nat Commun. 2024;15(1):3520.
31. Liu J, Chu G, Wang Q, Zhang Z, Lu S, She Z, Zhao Y, Jin C, Guo L, Ji J, et al. Metagenomic analysis and nitrogen removal performance evaluation of activated sludge from a sequencing batch reactor under different salinities. J Environ Manage. 2022;323:116213.
32. Kumar, Lokesh, Futschik, Matthias. Mfuzz: A software package for soft clustering of microarray data. Bioinformation. 2007;2(1):5–7.
33. Zhang G, Zhao F, Chen L, Pan Y, Sun L, Bao N, Zhang T, Cui C-X, Qiu Z, Zhang Y, et al. Jasmonate-mediated wound signalling promotes plant regeneration. Nature Plants. 2019;5(5):491–7.
34. Fetzer I, Johst K, Schawe R, Banitz T, Chatzinotas A. The extent of functional redundancy changes as species' roles shift in different environments. Proc Natl Acad Sci. 2015;112(48):14888–93.
35. Liu S-J, Zhang H, Jin X-T, Niu M-X, Feng C-H, Liu X, Liu C, Wang H-L, Yin W, Xia X. PeFUS3 Drives Lateral Root Growth Via Auxin and ABA Signalling Under Drought Stress in Populus. Plant Cell Environ. 2025;48:664–81.
36. Li D, Yang J, Pak S, Zeng M, Sun J, Yu S, He Y, Li C. PuC3H35 confers drought tolerance by enhancing lignin and proanthocyanidin biosynthesis in the roots of Populus ussuriensis. New Phytol. 2021;233(1):390–408.
37. Xu W, Wang Y, Xie J, Tan S, Wang H, Zhao Y, Liu Q, El-Kassaby YA, Zhang D. Growth-regulating factor 15-mediated gene regulatory network enhances salt tolerance in poplar. Plant Physiol. 2022;191(4):2367–84.
38. Wang LQ, Wen SS, Wang R, Wang C, Gao B, Lu MZ. PagWOX11/12a activates PagCYP736A12 gene that facilitates salt tolerance in poplar. Plant Biotechnol J. 2021;19(11):2249–60.
39. Chen S, Tan S, Jin Z, Wu J, Zhao Y, Xu W, Liu S, Li Y, Huang H, Bao F, et al. The transcriptional landscape of Populus pattern/effector-triggered immunity and how PagWRKY18 involved in it. Plant Cell Environ. 2024;47(6):2074–92.
40. Yang Y, Li H-G, Liu M, Wang H-L, Yang Q, Yan D-H, Zhang Y, Li Z, Feng C-H, Niu M, et al. PeTGA1 enhances disease resistance against Colletotrichum gloeosporioides through directly regulating PeSARD1 in poplar. Int J Biol Macromol. 2022;214:672–84.
41. Vellend. Conceptual synthesis in community ecology. Q Rev Biol. 2010;2010,85(2)(-):183–206.
42. Wagg C, Schlaeppi K, Banerjee S, Kuramae EE, van der Heijden MGA. Fungal-bacterial diversity and microbiome complexity predict ecosystem functioning. Nat Commun. 2019;10(1):4841.
43. Jiao S, Chen W, Wei G. Core microbiota drive functional stability of soil microbiome in reforestation ecosystems. Glob Change Biol. 2022;28:1038–47.
44. Fierer N, Lennon JT. The generation and maintenance of diversity in microbial communities. Am J Bot. 2011;98(3):439–48.
45. Shi S, Nuccio EE, Shi ZJ, He Z, Zhou J, Firestone MK, Johnson N. The interconnected rhizosphere: High network complexity dominates rhizosphere assemblages. Ecol Lett. 2016;19(8):926–36.
46. Hernandez DJ, David AS, Menges ES, Searcy CA, Afkhami ME. Environmental stress destabilizes microbial networks. ISME J. 2021;15(6):1722–34.
47. Qiu L, Zhang Q, Zhu H, Reich PB, Banerjee S, van der Heijden MGA, Sadowsky MJ, Ishii S, Jia X, Shao M, et al. Erosion reduces soil microbial diversity, network complexity and multifunctionality. ISME J. 2021;15(8):2474–89.
48. Li C, Jin L, Zhang C, Li S, Zhou T, Hua Z, Wang L, Ji S, Wang Y, Gan Y, et al. Destabilized microbial networks with distinct performances of abundant and rare biospheres in maintaining networks under increasing salinity stress. iMeta. 2023;2(1):e79.
49. Berendsen RL, Vismans G, Yu K, Song Y, de Jonge R, Burgman WP, Burmølle M, Herschend J, Bakker PAHM, Pieterse CMJ. Disease-induced assemblage of a plant-beneficial bacterial consortium. ISME J. 2018;12(6):1496–507.
50. Dudenhöffer JH, Scheu S, Jousset A, Cahill J. Systemic enrichment of antifungal traits in the rhizosphere microbiome after pathogen attack. J Ecol. 2016;104(6):1566–75.
51. Kong HG, Kim BK, Song GC, Lee S, Ryu C-M. Aboveground Whitefly Infestation-Mediated Reshaping of the Root Microbiota. Front Microbiol. 2016;7:1314.
52. Berendsen RL, Vismans G, Yu K, Song Y, De Jonge R, Burgman WP, et al. Disease-induced assemblage of a plant-beneficial bacterial consortium. Isme J. 2018;12:1496–507.
53. Yuan J, Zhao J, Wen T, et al. Root exudates drive the soil-borne legacy of aboveground pathogen infection. Microbiome. 2018;6:156.
54. Gao M, Xiong C, Gao C, Tsui CKM, Wang M-M, Zhou X, Zhang A-M, Cai L. Disease-induced changes in plant microbiome assembly and functional adaptation. Microbiome. 2021;9(1):187.
55. Lau, JA, Lennon JT. Rapid responses of soil microorganisms improve plant fitness in novel environments. P NATL ACAD SCI USA. 2012:2012,109(35)(-):14058–14062.
56. Castrillo G, Teixeira PJPL, Paredes SH, Law TF, de Lorenzo L, Feltcher ME, Finkel OM, Breakfield NW, Mieczkowski P, Jones CD, et al. Root microbiota drive direct integration of phosphate stress and immunity. Nature. 2017;543(7646):513–8.
57. Tuang ZK, Wu Z, Jin Y, Wang Y, Oo PPZ, Zuo G, Shi H, Yang W. Pst DC3000 infection alleviates subsequent freezing and heat injury to host plants via a salicylic acid-dependent pathway in Arabidopsis. Plant, Cell Environ. 2020;43(3):801–17.
58. Suzuki N, Rivero RM, Shulaev V, Blumwald E, Mittler R. Abiotic and biotic stress combinations. New Phytol. 2014;203(1):32–43.
59. Mueller UG, Linksvayer TA. Microbiome breeding: conceptual and practical issues. Trends Microbiol. 2022;30(10):997–1011.
60. Cernava T. Coming of age for Microbiome gene breeding in plants. Nat Commun. 2024;15(1):6623.
61. Su P, Kang H, Peng Q, Wicaksono WA, Berg G, Liu Z, Ma J, Zhang D, Cernava T, Liu Y. Microbiome homeostasis on rice leaves is regulated by a precursor molecule of lignin biosynthesis. Nat Commun. 2024;15(1):23.
62. Escudero-Martinez C, Coulter M, Alegria Terrazas R, Foito A, Kapadia R, Pietrangelo L, Maver M, Sharma R, Aprile A, Morris J, et al. Identifying plant genes shaping microbiota composition in the barley rhizosphere. Nat Commun. 2022;13(1):3443.

63. Oyserman BO, Flores SS, Griffioen T, Pan X, van der Wijk E, Pronk L, Lokhorst W, Nurfikari A, Paulson JN, Movassagh M, et al. Disentangling the genetic basis of rhizosphere microbiome assembly in tomato. Nat Commun. 2022;13(1):3228.
64. Liu H, Brettell LE. Plant Defense by VOC-Induced Microbial Priming. Trends Plant Sci. 2019;24(3):187–9.
65. Canarini A, Kaiser C, Merchant A, Richter A, Wanek W. Root Exudation of Primary Metabolites: Mechanisms and Their Roles in Plant Responses to Environmental Stimuli. Front Plant Sci. 2019;10:157.
66. Rudrappa T, Czymmek KJ, Paré PW, Bais HP. Root-Secreted Malic Acid Recruits Beneficial Soil Bacteria. Plant Physiol. 2008;148(3):1547–56.
67. Raaijmakers JM, Mazzola M. Diversity and Natural Functions of Antibiotics Produced by Beneficial and Plant Pathogenic Bacteria. Annu Rev Phytopathol. 2012;50(1):403–24.
68. Zhang L, Zhang M, Huang S, Li L, Gao Q, Wang Y, Zhang S, Huang S, Yuan L, Wen Y, et al. A highly conserved core bacterial microbiota with nitrogen-fixation capacity inhabits the xylem sap in maize plants. Nat Commun. 2022;13(1):3361.
69. Lauber CL, Strickland MS, Bradford MA, Noah F. The influence of soil properties on the structure of bacterial and fungal communities across land-use types. Soil Biol Biochem. 2008;9:40.
70. Defining the core Arabidopsis thaliana root microbiome. Nature. 2012;488(7409):86–90,A82.
71. Coyte KZ, Rakoff-Nahoum S. Understanding Competition and Cooperation within the Mammalian Gut Microbiome. Curr Biol. 2019;29(11):R538–44.
72. Yang Y, Cheng K, Li K, Jin Y, He X. Deciphering the diversity patterns and community assembly of rare and abundant bacterial communities in a wetland system. Sci Total Environ. 2022;838:156334.
73. Xu M, Huang Q, Xiong Z, Liao H, Lv Z, Chen W, Luo X, Hao X, Hug LA. Distinct Responses of Rare and Abundant Microbial Taxa to In Situ Chemical Stabilization of Cadmium-Contaminated Soil. mSystems. 2021;6(5):e01040–21.
74. Xiong C, He JZ, Singh BK, Zhu YG, Wang JT, Li PP, Zhang QB, Han LL, Shen JP, Ge AH, et al. Rare taxa maintain the stability of crop mycobiomes and ecosystem functions. Environ Microbiol. 2020;23(4):1907–24.
75. He Z, Liu D, Shi Y, Wu X, Dai Y, Shang Y, Peng J, Cui Z. Broader environmental adaptation of rare rather than abundant bacteria in reforestation succession soil. Sci Total Environ. 2022;828:154364.
76. He J, Zhang N, Muhammad A, Shen X, Sun C, Li Q, Hu Y, Shao Y. From surviving to thriving, the assembly processes of microbial communities in stone biodeterioration: A case study of the West Lake UNESCO World Heritage area in China. Sci Total Environ. 2022;805:150395.
77. Xu Q, Vandenkoornhuyse P, Li L, Guo J, Zhu C, Guo S, Ling N, Shen Q. Microbial generalists and specialists differently contribute to the community diversity in farmland soils. J Adv Res. 2022;40:17–27.
78. Graham E, Stegen J. Dispersal-Based Microbial Community Assembly Decreases Biogeochemical Function. Processes. 2017;5(4):65.
79. Xun W, Li W, Xiong W, Ren Y, Liu Y, Miao Y, Xu Z, Zhang N, Shen Q, Zhang R. Diversity-triggered deterministic bacterial assembly constrains community functions. Nat Commun. 2019;10(1):3833.
80. Goldford JE, Lu N, Bajic D, Estrela S, Tikhonov M, Sanchez-Gorostiaga A, Segre D, Mehta P, Sanchez A. Emergent Simplicity in Microbial Community Assembly. ence. 2018;361(6401):469–474.
81. Naeem S. Ecosystem consequences of biodiversity loss: the evolution of a paradigm. Ecology. 2002;83(6):1537–52.
82. Loreau M. Biodiversity and ecosystem functioning: A mechanistic model. Proc Natl Acad Sci. 1998;95(10):5632–6.
83. Jax. Function and functioning in ecology: what does it mean? OIKOS. 2005;111:641–8.
84. Cardinale BJ. Biodiversity improves water quality through niche partitioning. Nature. 2011;472(7341):86–9.
85. Lewis WH, Tahon G, Geesink P, Sousa DZ, Ettema TJG. Innovations to culturing the uncultured microbial majority. Nat Rev Microbiol. 2020;19(4):225–40.
86. Zhang J, Liu Y-X, Guo X, Qin Y, Garrido-Oter R, Schulze-Lefert P, Bai Y. High-throughput cultivation and identification of bacteria from the plant root microbiota. Nat Protoc. 2021;16(2):988–1012.
87. Wei Z, Gu Y, Friman VP, Kowalchuk GA, Jousset A. Initial Soil Microbiome Composition and Functioning Predetermine Future Plant Health. Sci Adv. 2019;5(9):eaaw0759.
88. Weir BS, Johnston PR, Damm U. The Colletotrichum gloeosporioides species complex. Stud Mycol. 2012;73(1):115–80.
89. Martiny JBH, Jones SE, Lennon JT, Martiny AC. Microbiomes in light of traits: A phylogenetic perspective. Science. 2015;350:6261.
90. Newman MEJ. The structure and function of complex networks. Siam Review. 2003;45:167–256.
91. Barberán A, Bates ST, Casamayor EO, Fierer N. Using network analysis to explore co-occurrence patterns in soil microbial communities. ISME J. 2012;6(2):343–51.
92. Li P-D, Zhu Z-R, Zhang Y, Xu J, Wang H, Wang Z, Li H. The phyllosphere microbiome shifts toward combating melanose pathogen. Microbiome. 2022;10(1):56.
93. Pikovskaya RI. Mobilization of phosphorus in soil in connection with the vital activity of some microbial species. Mikrobiologiya. 1948;17:362–70.
94. Patil CD, Mohite BV, Suryawanshi RK, Patil SV. Isolation and Screening of Silicate Solubilizing Microbes: Modern Bioinputs for Crops. Practical Handbook on Agricultural Microbiology. Springer Protocols Handbooks. 2022;237–42.
95. Andrews MYS, Cara M.Duckworth, Owen W. Layer plate CAS assay for the quantitation of siderophore production and determination of exudation patterns for fungi. J Microbiol Methods. 2016;121:41–3.
96. Gordon SA, Weber RP. Colorimetric estimation of indoleacetic acid. Plant Physiol. 1951;26(1):192–5.

Publisher's Note